

Blood-Capillary-Inspired, Free-Standing, Flexible, and Low-Cost Super-Hydrophobic N-CNTs@SS Cathodes for High-Capacity, High-Rate, and Stable Li-Air Batteries

Xiao-Yang Yang, Ji-Jing Xu, Zhi-Wen Chang, Di Bao, Yan-Bin Yin, Tong Liu, Jun-Min Yan, Da-Peng Liu, Yu Zhang,* and Xin-Bo Zhang

With the rising demand for flexible and wearable electronic devices, flexible power sources with high energy densities are required to provide a sustainable energy supply. Theoretically, rechargeable, flexible Li-O₂/air batteries can provide extremely high specific energy densities; however, the high costs, complex synthetic methods, and inferior mechanical properties of the available flexible cathodes severely limit their practical applications. Herein, inspired by the structure of human blood capillary tissue, this study demonstrates for the first time the in situ growth of interpenetrative hierarchical N-doped carbon nanotubes on the surface of stainless-steel mesh (N-CNTs@SS) for the fabrication of a self-supporting, flexible electrode with excellent physico-chemical properties via a facile and scalable one-step strategy. Benefitting from the synergistic effects of the high electronic conductivity and stable 3D interconnected conductive network structure, the Li-O₂ batteries obtained with the N-CNTs@SS cathode exhibit superior electrochemical performance, including a high specific capacity (9299 mA h g⁻¹ at 500 mA g⁻¹), an excellent rate capability, and an exceptional cycle stability (up to 232 cycles). Furthermore, as-fabricated flexible Li-air batteries containing the as-prepared flexible super-hydrophobic cathode show excellent mechanical properties, stable electrochemical performance, and superior H₂O resistibility, which enhance their potential to power flexible and wearable electronic devices.

The number of electronic devices with flexible, wearable, and portable features has risen exponentially in recent years, and these devices have received increasing attention regarding their promising practical applications as wearable electronics, roll-up displays, intelligent devices, and wireless sensors.^[1–6] As a result, there is a high demand for the development of high-density, flexible energy storage systems to power them. Recently, tremendous efforts have been made to develop flexible lithium-ion batteries,^[7–10] sodium-ion batteries,^[11] supercapacitors,^[12–14] and solar cells.^[15–17] However, these systems are still limited by low theoretical energy densities. To meet the increasing demand for intelligent devices, the development of flexible energy storage systems with high energy densities is extremely urgent.

Metal-air batteries have been studied as promising energy storage systems for next-generation wearable devices owing to their low cost, environmental friendliness, and especially high energy densities.^[18–20]

In particular, Li-air batteries, promising systems in the field of metal-air batteries, possess the highest theoretical capacity density and have attracted increasing attention in recent years.^[21–25] However, currently, most of the cathodes used in Li-O₂/air batteries are bulky and rigid and cannot meet the required portability and flexibility for the design of flexible Li-O₂/air battery devices. In response, efforts have been made to construct flexible cathodes based on carbon cloth,^[26,27] carbon fiber,^[28] and aligned carbon nanotube (CNT) sheets.^[29] To a certain extent, these studies have provided feasible schemes for the construction of flexible cathodes. Nevertheless, the inferior properties, including low mechanical strength and poor electrochemical properties, of the available cathodes cannot satisfy the requirements of flexible and wearable Li-O₂/air batteries. Furthermore, complex synthetic methods, harsh preparation conditions and high prices have prevented them from being available on the market. Theoretically, CNTs with hierarchical and fibrous structures can serve desired cathode materials for Li-O₂/air batteries.^[30] However, the synthesis of CNTs often requires rigorous experimental conditions, and the addition of combustible reaction gases (e.g., C₂H₄ and CH₄) also leads to serious hidden dangers. In general, CNTs

X.-Y. Yang, J.-J. Xu, Z.-W. Chang, Dr. D. Bao, Y.-B. Yin, T. Liu, Prof. X.-B. Zhang

State Key Laboratory of Rare Earth Resource Utilization
Changchun Institute of Applied Chemistry
Chinese Academy of Sciences
Changchun 130022, P. R. China

X.-Y. Yang, Y.-B. Yin, Prof. J.-M. Yan
Key Laboratory of Automobile Materials
Ministry of Education
Department of Materials Science and Engineering
Jilin University
Changchun 130022, P. R. China

Z.-W. Chang, T. Liu
University of Chinese Academy of Sciences
Beijing 100049, P. R. China

Dr. D.-P. Liu, Prof. Y. Zhang
Key Laboratory of Bio-Inspired Smart Interfacial Science
and Technology of Ministry of Education
School of Chemistry and Environment
Beihang University
Beijing 100191, P. R. China
E-mail: jade@buaa.edu.cn

DOI: 10.1002/aenm.201702242

are closely aggregated by a binder in traditional CNT-based air electrodes, and such tightly aggregated structures with small pore sizes and volumes cannot provide a sufficient amount of effective spaces to store large amounts of discharge products. Moreover, the lack of interconnected channels and barriers in the polymeric binders also lead to a low utilization ratio of the CNTs and poor battery performance, including poor rate capabilities and low specific capacities.^[31–33] Therefore, it is very necessary to design and fabricate a cost-efficient, binder-free, and self-supporting flexible CNT cathode with excellent electrochemical and mechanical properties via a simple method.

Human blood capillary tissue possesses unique interpenetrative structures that can provide sufficient space and a high diffusion area to facilitate the efficient transport of oxygen and nutrition to organisms. The above structural features are also significant for the ability of Li-O₂ batteries to store the discharge products and realize the fast transport of electrons and gas. Herein, inspired by blood capillary tissue, we demonstrate for the first time the in situ growth of N-doped CNTs on the surface of a stainless-steel mesh (N-CNTs@SS) for the fabrication of a self-supporting, flexible air electrode with an interpenetrative structure via a facile and scalable one-step strategy. Owing to the unique physical properties of the stainless-steel mesh (SS) substrate, an electrode with excellent mechanical properties and strength was prepared. The hierarchical and controlled porous framework of the N-CNTs can provide a sufficient number of spaces to accommodate the insoluble discharge products and subsequently prevent degeneration of the pores due to the discharge products, even during deep discharge. Significantly, the interpenetrative networks provide abundant crosslinked channels that facilitate the transport of both electrons and gas through the cathode. With the synergistic effects of the above advantages, the N-CNTs@SS exhibit superior electrochemical performance, including a high specific capacity, excellent rate capability, and especially good cycle stability. Surprisingly, the N-CNTs@SS cathode manifests super hydrophobicity, enabling the achievement of a safe and long-life Li-air battery for us in humid atmospheres.

The fabrication of self-supporting N-CNTs@SS is illustrated in Figure S1 (Supporting Information). Via a simple one-step synthetic process, N-CNTs were grown in situ on the SS surface using ferrum particles as the precatalyst and melamine as the nitrogen and carbon source in an atmospheric pressure tube furnace with an Ar gas flow under different temperatures. The as-prepared N-CNTs@SS cathode is shown in Figure S2a (Supporting Information) and exhibits superior flexibility even at a torsion angle of 360° (Figure S2b, Supporting Information). Scanning electron microscopy (SEM) was used to initially characterize the structure and morphological evolution. As shown in Figure 1a–c, the final annealing temperature significantly affected the morphology of the products and led to a different electrode structure. When we maintained the final temperature at 700 °C, only carbon particles and very few short irregular nanotubes were observed on the SS surface (Figure 1a). Conversely, upon increasing the temperature to 750 °C, N-CNTs with a uniform morphology dominated the product (Figure 1b). The interpenetrative N-CNTs were loosely packed on the SS surface and organized in a hierarchical structure with a large amount of free internal spaces, which could facilitate both gas

transport and facile electron transport through the network. However, when the temperature was increased to 800 °C, the heterogeneous nanotubes exhibited an imperfect structure (Figure 1c). The structures of the final products synthesized under different temperatures were then investigated by X-ray diffraction (XRD). A carbon peak emerged when the temperature was increased to 750 °C. Upon further increasing the temperature, the position and intensity of the carbon peak did not distinctly change (Figure 1d). The Raman spectra of the N-CNTs@SS samples synthesized under different temperatures were also plotted for comparison (Figure S3, Supporting Information). All of the spectra consisted of two strong peaks at 1351 and 1580 cm⁻¹, corresponding to the D and G bands, respectively, of the N-CNTs.^[34] Considering the above aspects, we selected the N-CNTs@SS synthesized at 750 °C as the final product. X-ray photoelectron spectroscopy (XPS) was performed for the surface elemental analysis of the N-CNTs@SS synthesized at 750 °C. The XPS spectrum shown in Figure S4 (Supporting Information) clearly reveals that carbon, nitrogen, and oxygen were present on the surface of the N-CNTs. As shown in the high-resolution C 1s spectrum, the peaks at 284.6, 285.2, 287.3, and 289.0 eV can be assigned to carbon in the forms of C–C (sp³), C–N (sp³), C=O (sp²), and O–C=O (sp²), respectively (Figure 1e).^[35] The high-resolution N 1s spectrum was also obtained to confirm the successful incorporation of nitrogen and to determine the types of nitrogen in the N-CNTs. The N 1s spectrum reveals that the typical N groups included pyridinic, pyrrolic, and graphitic N species (Figure 1f).^[36] The transmission electron microscopy (TEM) results reveal a hollow multiwall nanotube structure with an inner diameter of 20 nm (Figure 1g). The nitrogen adsorption/desorption isotherm illustrates the mesoporous features of the N-CNTs, with a Brunauer–Emmett–Teller surface area of 156.7 m² g⁻¹ (Figure S5, Supporting Information). The high-resolution TEM images show a distinct lattice spacing of 0.335 nm for the multilayered shell structure, which is consistent with the (400) lattice plane of the carbon product (Figure S6, Supporting Information).^[37] Moreover, energy dispersive X-ray spectroscopy (EDS) element mapping confirmed that the carbon and nitrogen in the N-CNTs networks were homogeneously distributed on the SS surface (Figure 1h).

Considering the good electrical conductivity and high mechanical strength of the SS substrate, we then investigated the physical and mechanical properties of the N-CNTs@SS cathode. Unsurprisingly, the as-prepared N-CNTs@SS cathode also had an excellent electronic conductivity of 896.5 S cm⁻¹, which is much higher than those of other carbon-based current collectors and CNT-based flexible materials, including carbon paper (46.73 S cm⁻¹), carbon cloth (33.15 S cm⁻¹), macroporous active carbon fiber (MACF) (3.3 S cm⁻¹),^[38] self-assembled multiwall CNTs (2.5 S cm⁻¹), and activated carbon nanofibers (0.22 S cm⁻¹) (Figure S7, Supporting Information). In addition, for flexible cathodes, high mechanical strength is an essential requirement. The as-prepared N-CNTs@SS had a very high tensile strength of 68.5 MPa (Figure S8, Supporting Information), which is much higher than those of the conventional flexible materials used in Li-O₂/air batteries, such as carbon cloth (5.71 MPa) and carbon nanofibers (12.0 MPa) (Figure S9, Supporting Information). More

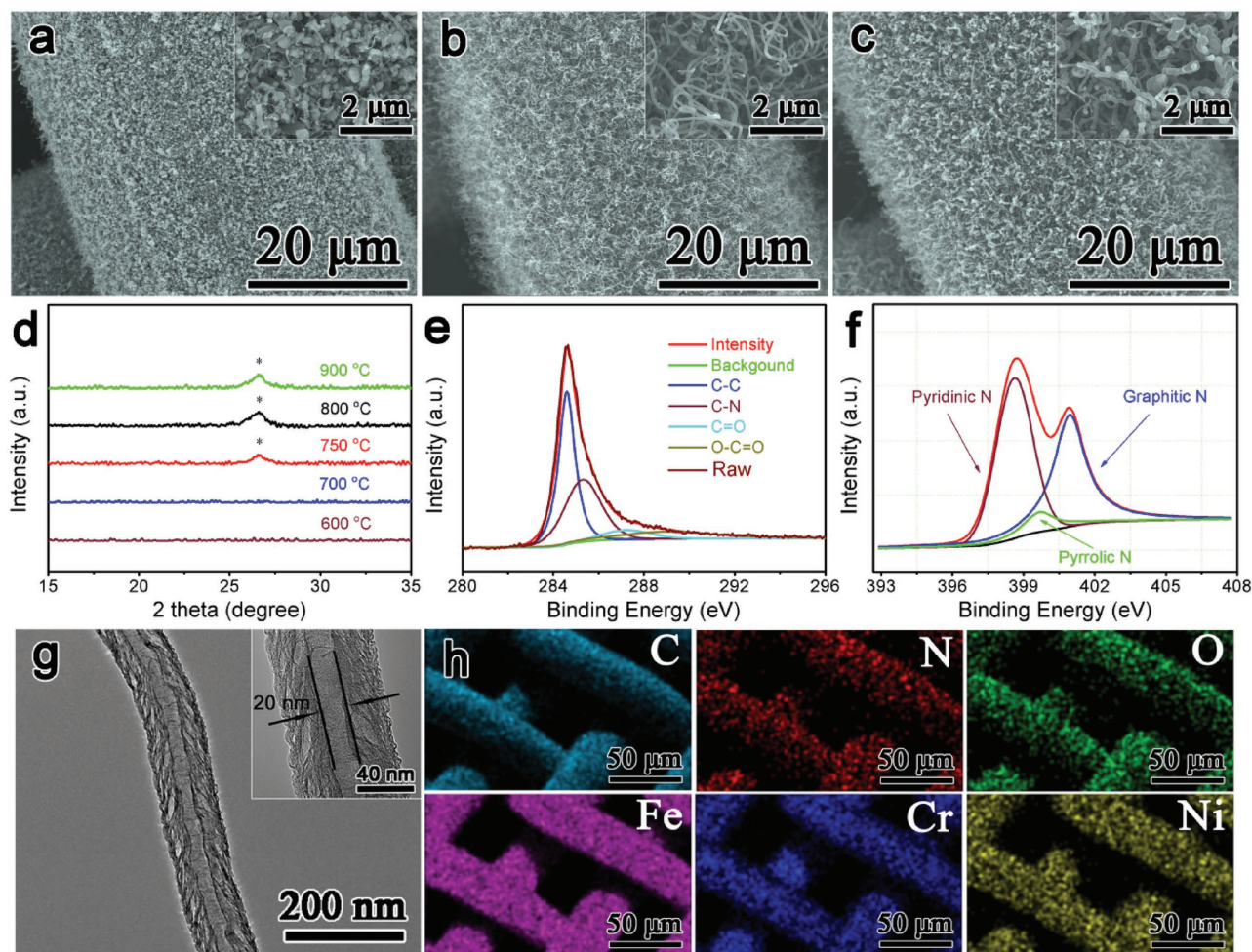


Figure 1. a–c) SEM images of the N-CNTs@SS samples synthesized at 700, 750, and 800 °C, respectively (insets are enlarged SEM images), d) XRD patterns of the N-CNTs@SS samples synthesized at different temperatures; high-resolution. e) C 1s and f) N 1s XPS spectra of the resultant N-CNTs@SS, g) TEM image of an N-CNT (inset is an enlarged image of the tube), h) SEM EDS elemental mapping of C, N, O, Fe, Cr, and Ni of the N-CNTs@SS.

importantly, contact angle (CA) measurements show that the N-CNTs@SS cathode is super-hydrophobic, with a water CA of 150° (Figure S10a, Supporting Information), which is significant for most of the nonaqueous energy storage systems, such as lithium batteries and supercapacitors.^[39] Moreover, the super-hydrophobic properties of the N-CNTs@SS cathode prevented H₂O crossover toward the Li metal anode (Video S1, Supporting Information), which endowed the battery with resistance against H₂O and improved the safety coefficient.^[27,40] Surprisingly, when the droplets were changed from H₂O to tetraethylene glycol dimethyl ether, the obtained N-CNTs@SS was lipophilic, with a CA of 0° (Figure S10b, Supporting Information). The lipophilicity of the N-CNTs@SS caused the formation of uniform solid–liquid–gas regions, ensured the full utilization of the active area of the cathode, and in turn facilitated the distribution and flux of both the reactants and electrolyte during the battery reactions.

Owing to the successful imitation of the superior morphology and structure of blood capillary tissue and inspired by the above advantages of the N-CNTs@SS, as a proof-of-concept application, we utilized the N-CNTs@SS as an Li-O₂ battery cathode.

For comparison, commercial CNTs and N-CNTs were also utilized. At a discharge current density of 500 mA g⁻¹ with a cutoff voltage of 2.3 V, the N-CNTs@SS cathode delivered a higher discharge capacity (9299 mA h g⁻¹) than the cathodes synthesized at 700 °C (4825 mA h g⁻¹) and 800 °C (5454 mA h g⁻¹), the commercial CNTs (5687 mA h g⁻¹), and the commercial N-CNTs (6415 mA h g⁻¹) (Figure 2a). The following rate performance investigations show that the discharge voltage plateau of the N-CNTs@SS cathode was higher than that of the commercial CNT and N-CNT cathodes at each current density (Figure 2b). The specific capacities at different current densities are also provided to demonstrate the excellent rate capability of the N-CNTs@SS cathode (Figure 2c). It is worth noting that the achieved superior rate capability was attributed to the following synergetic advantages of the N-CNTs@SS cathode: (i) the high electronic conductivity and interconnected channels within the cathode could provide a “highway” for charge transfer; (ii) the interpenetrative and hierarchical structure could prevent clogging of the channels by the discharge product and ensure the diffusion of Li⁺ and O₂ with high efficiency; and (iii) the doped N could promote electrocatalytic activity.^[41,42]

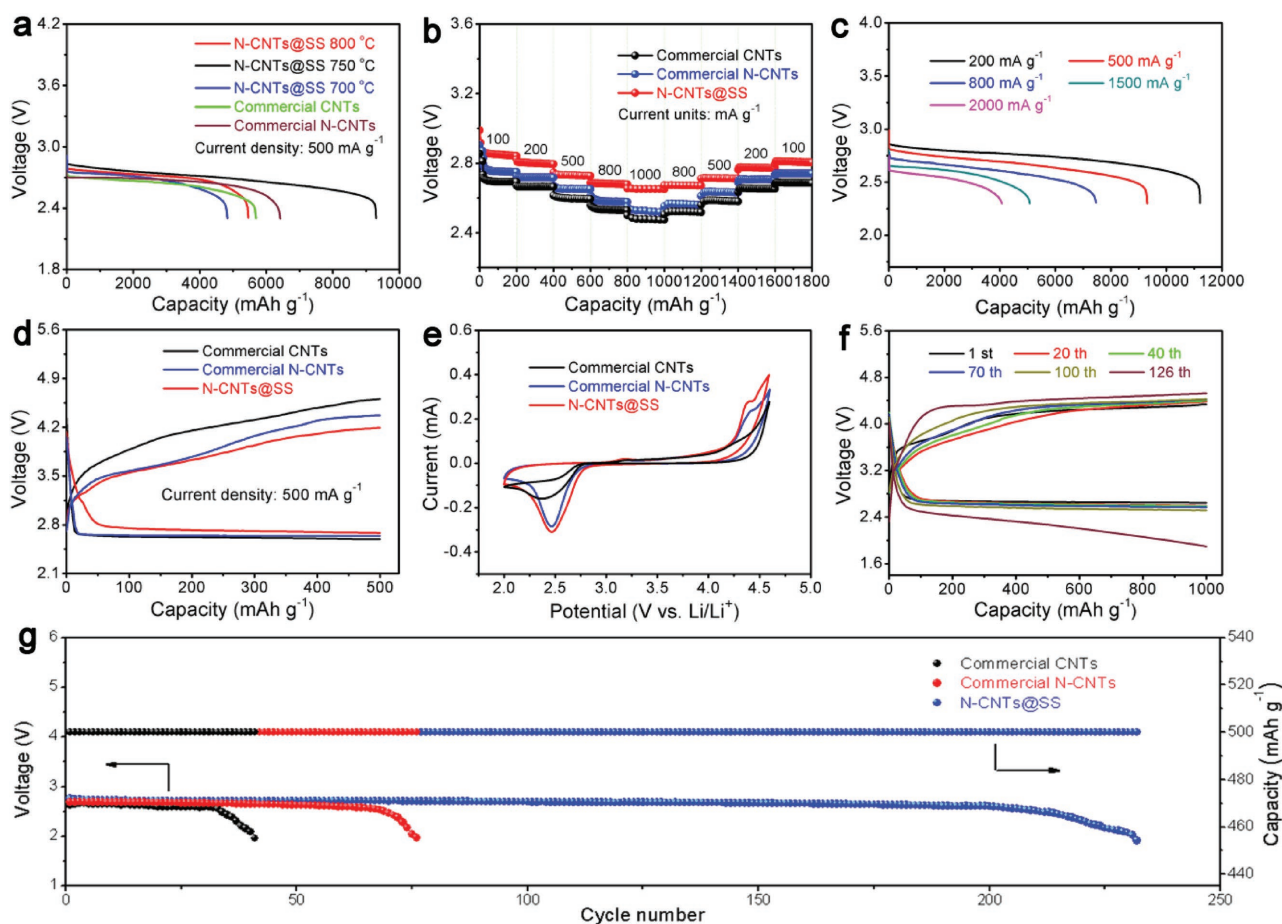


Figure 2. a) The discharge capacity of Li-O₂ batteries with five different cathodes at a current density of 500 mA g⁻¹, b) the rate capability of Li-O₂ batteries with three types of cathodes, c) the discharge capacity of Li-O₂ batteries with N-CNTs@SS cathodes at various current densities, d) the first discharge–charge curves of Li-O₂ batteries with three different cathodes, e) CVs of Li-O₂ batteries with three types of cathodes at a constant scan rate of 0.1 mV s⁻¹, f) the cycle performance of N-CNTs@SS at a current density of 500 mA g⁻¹ and a specific capacity limited to 1000 mA h g⁻¹, g) the terminal discharge voltage of Li-O₂ batteries with the three different cathodes at a current density of 500 mA g⁻¹.

The discharge–charge overpotentials of the Li-O₂ battery with the N-CNT@SS cathode (0.62 and 0.35 V, respectively) were lower than those of the commercial CNT and N-CNT cathodes (Figure 2d). The electrochemical performance of the three types of cathodes was further investigated by cyclic voltammetry (CV) at a constant scan rate of 0.1 mV s⁻¹ (Figure 2e). The first cycle curve reveals that the N-CNTs@SS cathode exhibited a more positive oxygen reduction reaction onset potential and a more negative oxygen evolution reaction onset potential than the other cathodes. These results reveal that the N-CNTs@SS exhibit superior electrochemical performance in both the formation and decomposition of the discharge products.^[23] After 123 cycles, the terminal discharge voltage was still above 2.0 V for the Li-O₂ battery with the N-CNTs@SS cathode, with the capacity limited to 1000 mA h g⁻¹ at a current density of 500 mA g⁻¹ (Figure 2f). Furthermore, with the capacity limited to 500 mA h g⁻¹, the Li-O₂ battery with the N-CNTs@SS cathode was stable for up to 232 cycles. In sharp contrast, the Li-O₂ batteries with the commercial CNT and N-CNTs cathodes were only stable for up to 41 and 76 cycles, respectively, under the same conditions.

Exploring the formation and decomposition processes of the discharge products is crucial for understanding the electrochemical behavior of Li-O₂ batteries. XRD and Fourier transform infrared (FTIR) spectroscopy were conducted to identify the discharge products of the Li-O₂ batteries with N-CNTs@SS cathodes. Only the characteristic peaks of Li₂O₂ were observed in the XRD pattern after the first discharge process (Figure S11, Supporting Information).^[43] The characteristic peaks of Li₂O₂ were also observed in the obtained FTIR spectra (Figure S12, Supporting Information).^[44] Furthermore, the galvanostatic intermittent titration technique measurement^[45] indicated that the equilibrium discharge potential of the Li-O₂ battery was near 2.96 V, which is in accordance with the formation potential of Li₂O₂ (Figure S13, Supporting Information).^[46,47] Then, we utilized SEM to investigate the morphology and distribution of the discharge products on the cathode after the first discharge. The toroidal Li₂O₂ was well distributed along the N-CNTs (Figure 3a) and showed that the cathode provided uniform solid–liquid–gas regions for reactant diffusion and offered a sufficient number of spaces to accommodate the discharge products. More importantly, the hierarchical and interpenetrative structure of the

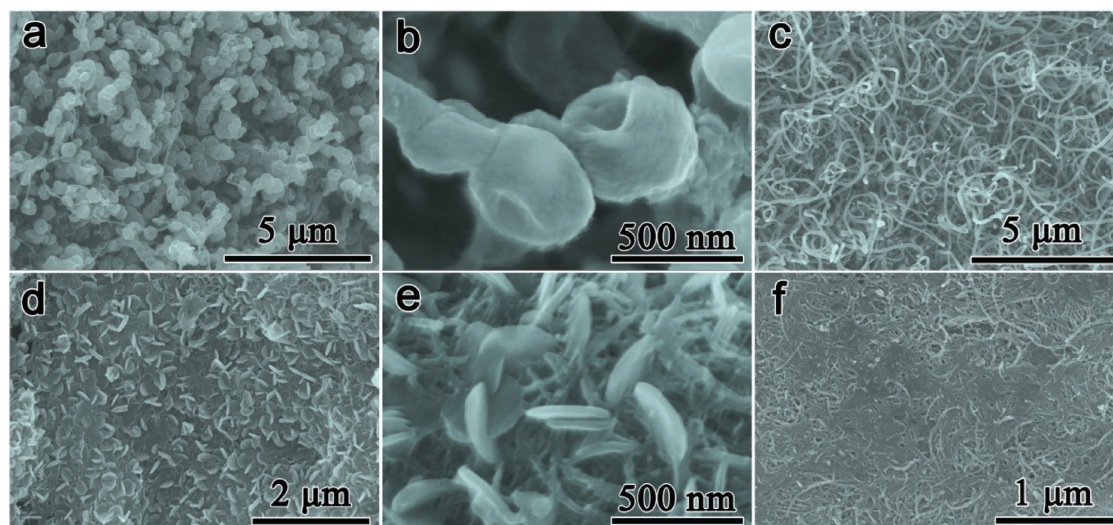


Figure 3. a) SEM image and b) enlarged image of the discharged N-CNTs@SS cathode with a cutoff voltage of 2.2 V, c) SEM image of the recharged N-CNTs@SS cathode, d) SEM image and e) enlarged image of the discharged commercial N-CNT cathode with a cutoff voltage of 2.2 V, f) SEM image of the recharged commercial N-CNT cathode.

cathode was maintained even after deep discharge (Figure 3a,b). After recharging, all of the discharge products disappeared, the N-CNTs@SS cathode recovered to its initial state, and the surface of the N-CNTs became smooth again (Figure 3c). The XRD patterns (Figure S11, Supporting Information) and FTIR spectra (Figure S12, Supporting Information) following the first discharge and recharge of the N-CNT@SS cathode also revealed the formation and decomposition of Li_2O_2 . All of the above results demonstrate the high reversibility of the Li- O_2 battery with the N-CNTs@SS cathode. Furthermore, the pristine structure of the N-CNTs@SS cathode was maintained even after multiple cycles (20, 40, 60, and 80 cycles) (Figure S14, Supporting Information), which demonstrates the good structural stability of the N-CNTs@SS cathode. In contrast, on the surface of the commercial CNTs cathode, the slurry and toroidal discharge products exhibited a disordered distribution (Figure 3d). The insoluble and insulating discharge products substantially blocked the channels and pores (Figure 3e), finally leading to destruction of the electrode structure after recharging (Figure 3f).

Inspired by the urgent requirement for flexible batteries for portable and wearable electronic devices in recent years, we fabricated flexible, rechargeable, cable-type Li-air batteries using the N-CNTs@SS cathode. With the aim of employing this super-hydrophobic N-CNTs@SS cathode to achieve the operation of an Li-air battery in a humid atmosphere, a hydrophobic gel polymer electrolyte,^[27] and ionic liquid-based electrolyte (0.5 M LiTFSI dissolved in 1-methyl-3-propylimidazolium bis(trifluoromethylsulfonyl)imide) were incorporated. The as-fabricated cable-type Li-air batteries were intentionally twisted and bent into different shapes to investigate their flexibility. The red light-emitting diode (LED) display screen remained constantly lit under all the testing conditions (Figure 4a). Furthermore, the discharge curves and capacity values of the Li-air batteries with different shapes were not significantly changed at a current density of 200 mA g^{-1} (Figure 4b). The discharge-charge ability of the flexible Li-air batteries after

thousands of rounds of bending and stretching was investigated to demonstrate the stability of the battery under repeated bending (Figure 4c). The open-circuit voltage (OCV) was also recorded during consecutive ultimate bending processes. As shown in Figure 4d, the OCV remained nearly unchanged during bending from 0° to 180° . To explore the efficiency of the Li metal anode protection, the fabricated Li-air batteries were tested in a humid atmosphere with a relative humidity (RH) of 43%. For the Li-air battery with a commercial hydrophilic carbon cathode, the anode was seriously corroded with large amounts of LiOH on the surface of the Li metal after 30 cycles (Figure 4e). In the case of the N-CNTs@SS-based Li-air battery, although little LiOH formed (Figure 4f), the Li metal was effectively protected from H_2O corrosion. Encouragingly, the as-prepared flexible Li-air battery demonstrated a stable cycling performance for 121 cycles at a current density of 500 mA g^{-1} with a capacity limited to 1000 mA h g^{-1} under an air atmosphere (Figure S15, Supporting Information). All these results indicate the excellent mechanical properties, stable electrochemical performance, and superior H_2O resistibility of the flexible cable-type Li-air battery with the N-CNTs@SS cathode.

In summary, a low-cost, binder-free, and self-supporting flexible N-CNTs@SS cathode with a hierarchical structure and super-hydrophobic properties was successfully designed and fabricated for the first time through a simple one-step synthetic process. Owing to the successful imitation of the superior shape and structure of blood capillary tissue, the obtained N-CNTs@SS cathode exhibited excellent characteristics, including a suitable hierarchical structure, high electrical conductivity, superior mechanical strength and structural stability, facile synthesis, and low cost. As a proof-of-concept application, an Li- O_2 battery was obtained using the N-CNTs@SS electrode and showed superior electrochemical performance, including a high specific capacity, excellent rate capability, and good cycling performance. Furthermore, the N-CNTs@SS cathode-based, flexible, cable-type Li-air batteries displayed excellent mechanical properties, stable electrochemical performances, and superior H_2O resistibility, making

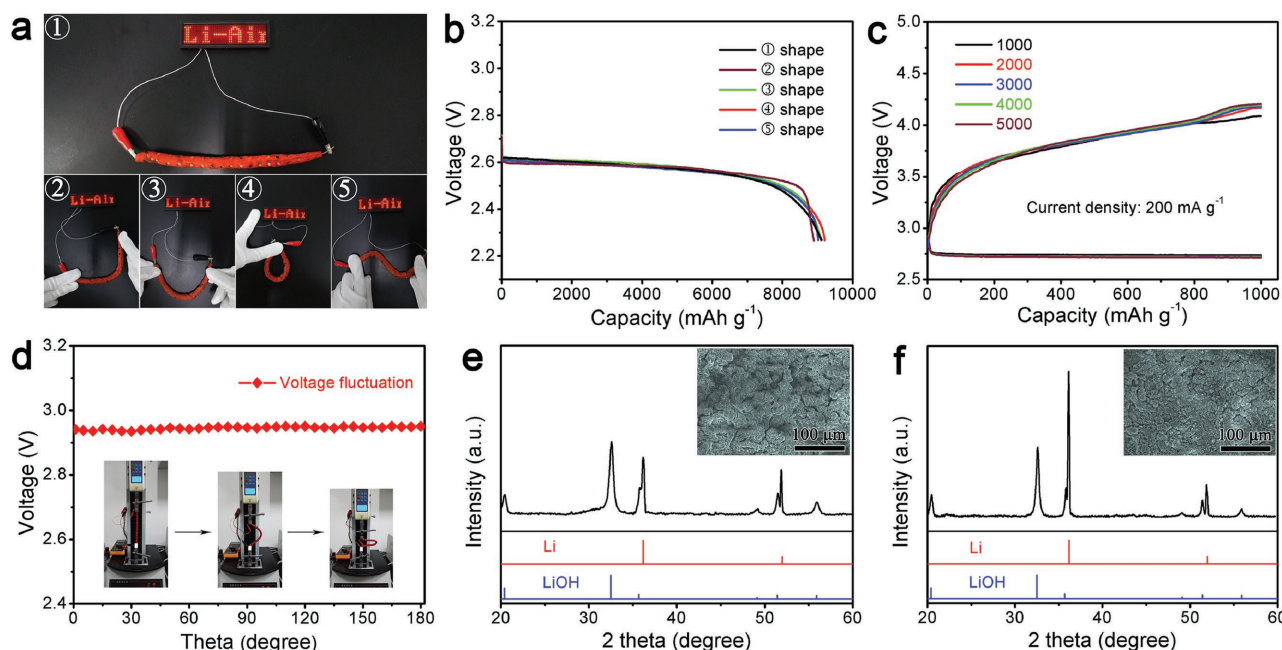


Figure 4. a) Cable-type flexible Li-air battery powering a commercial red LED display screen under various bent and twisted conditions and b) the corresponding discharge curves, c) charge–discharge curves of the cable-type, flexible, Li-air battery after thousands of rounds of bending, d) open-circuit voltage of the flexible Li-air battery during a continuous bending process from 0° to 180°; XRD patterns of the Li metal anodes after cycling at an RH of 43% of Li-air batteries assembled with e) a hydrophilic carbon cathode and f) the super-hydrophobic N-CNTs@SS cathode. The insets are the SEM images of corresponding Li metal anodes after cycling.

them promising for use in flexible electronic devices, which are severely restricted by the low theoretical energy densities of the existing flexible energy sources. We believe that this advanced biomimetic electrode design will provide great inspiration for further improvement of the electrochemical performance of Li-O₂/air batteries and other promising power systems.

Supporting Information

Supporting Information is available from the Wiley Online Library or from the author.

Acknowledgements

This work was financially supported by the National Natural Science Foundation of China (Grant Nos. 51522202, 51372007, 21422108, and 51472232, 21771013), the Specialized Research Fund for the Doctoral Program of Higher Education of China (20110061120040), and Jilin Province Science and Technology Development Program (Grant No. 20160101289JC).

Conflict of Interest

The authors declare no conflict of interest.

Keywords

biomimetics, cable-type, flexible, Li-O₂/air batteries, super-hydrophobic

Received: August 15, 2017
Revised: October 15, 2017
Published online: January 11, 2018

- [1] S. Park, G. Wang, B. Cho, Y. Kim, S. Song, Y. Ji, M. H. Yoon, T. Lee, *Nat. Nanotechnol.* **2012**, *7*, 438.
- [2] B. D. Gates, *Science* **2009**, *323*, 1566.
- [3] Y. Meng, Y. Zhao, C. Hu, H. Cheng, Y. Hu, Z. Zhang, G. Shi, L. Qu, *Adv. Mater.* **2013**, *25*, 2326.
- [4] Z. Liu, J. Xu, D. Chen, G. Shen, *Chem. Soc. Rev.* **2015**, *44*, 161.
- [5] L. Li, Z. Wu, S. Yuan, X.-B. Zhang, *Energy Environ. Sci.* **2014**, *7*, 2101.
- [6] S. W. Lee, N. Yabuuchi, B. M. Gallant, S. Chen, B. S. Kim, P. T. Hammond, Y. Shao-Horn, *Nat. Nanotechnol.* **2010**, *5*, 531.
- [7] M.-H. Park, K. Kim, J. Kim, J. Cho, *Adv. Mater.* **2010**, *22*, 415.
- [8] B. Liu, J. Zhang, X. Wang, G. Chen, D. Chen, C. Zhou, G. Shen, *Nano Lett.* **2012**, *12*, 3005.
- [9] X. Jia, Z. Chen, A. Suwarnasarn, L. Rice, X. Wang, H. Sohn, Q. Zhang, B. M. Wu, F. Wei, Y. Lu, *Energy Environ. Sci.* **2012**, *5*, 6845.
- [10] Y. Zhang, Y. Zhao, J. Ren, W. Weng, H. Peng, *Adv. Mater.* **2016**, *28*, 4524.
- [11] W. Zhang, Y. Liu, C. Chen, Z. Li, Y. Huang, X. Hu, *Small* **2015**, *11*, 3822.
- [12] Y. Meng, Y. Zhao, C. Hu, H. Cheng, Y. Hu, Z. Zhang, G. Shi, L. Qu, *Adv. Mater.* **2013**, *25*, 2326.
- [13] G. Qu, J. Cheng, X. Li, D. Yuan, P. Chen, X. Chen, B. Wang, H. Peng, *Adv. Mater.* **2016**, *28*, 3646.
- [14] H. Sun, S. Xie, Y. Li, Y. Jiang, X. Sun, B. Wang, H. Peng, *Adv. Mater.* **2016**, *28*, 8431.
- [15] D. Zhang, T. Yoshida, T. Oekermann, K. Furuta, H. Minoura, *Adv. Funct. Mater.* **2006**, *16*, 1228.
- [16] Z. Liu, J. Li, F. Yan, *Adv. Mater.* **2013**, *25*, 4296.

- [17] D. Liu, T. L. Kelly, *Nat. Photonics* **2014**, *8*, 133.
- [18] F. Cheng, J. Chen, *Chem. Soc. Rev.* **2011**, *41*, 2172.
- [19] J. Suntivich, H. A. Gasteiger, N. Yabuuchi, H. Nakanishi, J. B. Goodenough, S.-H. Yang, *Nat. Chem.* **2011**, *3*, 546.
- [20] Z.-L. Wang, D. Xu, J.-J. Xu, X.-B. Zhang, *Chem. Soc. Rev.* **2014**, *43*, 7746.
- [21] G. Girishkumar, B. McCloskey, A. C. Luntz, S. Swanson, W. Wilcks, *J. Phys. Chem. Lett.* **2010**, *1*, 2193.
- [22] P. G. Bruce, S. A. Freunberger, L. J. Hardwick, J.-M. Tarascon, *Nat. Mater.* **2012**, *11*, 19.
- [23] J.-J. Xu, Z.-L. Wang, D. Xu, L.-L. Zhang, X.-B. Zhang, *Nat. Commun.* **2013**, *4*, 2438.
- [24] L. Johnson, C. Li, Z. Liu, Y. Chen, S. A. Freunberger, P. C. Ashok, B. B. Praveen, K. Dholakia, J.-M. Tarascon, P. G. Bruce, *Nat. Chem.* **2014**, *6*, 1091.
- [25] T. Liu, M. Leskes, W. Yu, A. J. Moore, L. Zhou, P. M. Bayley, G. Kim, C. P. Grey, *Science* **2015**, *350*, 530.
- [26] Q.-C. Liu, J.-J. Xu, D. Xu, X.-B. Zhang, *Nat. Commun.* **2015**, *6*, 7892.
- [27] T. Liu, Q.-C. Liu, J.-J. Xu, X.-B. Zhang, *Small* **2016**, *12*, 3101.
- [28] Q.-C. Liu, T. Liu, D.-P. Liu, Z.-J. Li, X.-B. Zhang, Y. Zhang, *Adv. Mater.* **2016**, *28*, 8413.
- [29] Y. Zhang, L. Wang, Z. Guo, Y. Xu, Y. Wang, H. Peng, *Angew. Chem., Int. Ed.* **2016**, *55*, 4487.
- [30] H.-D. Lim, K.-Y. Park, H. Song, E. Y. Jang, H. Gwon, J. Kim, Y. H. Kim, M. D. Lima, R. O. Robles, X. Lepró, R. H. Baughman, K. Kang, *Adv. Mater.* **2013**, *25*, 1348.
- [31] P. Andrei, J. P. Zheng, M. Hendrickson, E. J. Plich, *J. Electrochem. Soc.* **2010**, *157*, A1287.
- [32] R. R. Mitchell, B. M. Gallant, C. V. Thompson, S.-H. Yang, *Energy Environ. Sci.* **2011**, *4*, 2952.
- [33] Z.-W. Chang, J.-J. Xu, Q.-C. Liu, L. Li, X.-B. Zhang, *Adv. Energy Mater.* **2015**, *5*, 1500633.
- [34] J. Fu, F. M. Hassan, J. Li, D. U. Lee, A. R. Ghannoum, G. Lui, M. A. Hoque, Z. Chen, *Adv. Mater.* **2016**, *28*, 6421.
- [35] Z. Yang, M. Xu, Y. Liu, F. He, F. Gao, Y. Su, H. Wei, Y. Zhang, *Nanoscale* **2014**, *6*, 1890.
- [36] W. Yang, X. Liu, X. Yue, J. Jia, S. Guo, *J. Am. Chem. Soc.* **2015**, *137*, 1436.
- [37] Z. Lu, W. Xu, J. Ma, Y. Li, X. Sun, L. Jiang, *Adv. Mater.* **2016**, *28*, 7155.
- [38] Y.-B. Yin, J.-J. Xu, Q.-C. Liu, X.-B. Zhang, *Adv. Mater.* **2016**, *28*, 7494.
- [39] M. M. O. Thotiyl, S. A. Freunberger, Z. Peng, P. G. Bruce, *J. Am. Chem. Soc.* **2013**, *135*, 494.
- [40] S. Wu, J. Yi, K. Zhu, S. Bai, Y. Liu, Y. Qiao, M. Ishida, H. Zhou, *Adv. Energy Mater.* **2017**, *7*, 1601759.
- [41] G. Wu, N. H. Mack, W. Gao, S. Ma, R. Zhong, J. Han, J. K. Baldwin, P. Zelenay, *ACS Nano* **2012**, *6*, 9764.
- [42] K. Zhang, L. Zhang, X. Chen, X. He, X. Wang, S. Dong, L. Gu, Z. Liu, C. Huang, G. Cui, *ACS Appl. Mater. Interfaces* **2013**, *5*, 3677.
- [43] B. D. Admas, C. Radtke, R. Black, M. L. Trudeau, K. Zaghbi, L. F. Nazar, *Energy Environ. Sci.* **2011**, *6*, 1772.
- [44] J.-J. Xu, Z.-W. Chang, Y. Wang, D.-P. Liu, Y. Zhang, X.-B. Zhang, *Adv. Mater.* **2016**, *28*, 9620.
- [45] T. Sasaki, Y. Ukyo, P. Novák, *Nat. Mater.* **2013**, *12*, 569.
- [46] H.-K. Lim, H.-D. Lim, K.-Y. Park, D.-H. Seo, H. Gwon, J. Hong, W. A. Goddard, H. Kim, K. Kang, *J. Am. Chem. Soc.* **2013**, *135*, 9733.
- [47] Z. H. Cui, X. X. Guo, H. Li, *Energy Environ. Sci.* **2015**, *8*, 182.